J. Appl. Comput. Mech., 12(3) (2026) 759-769
DOI: 10.22055/jacm.2025.48645.5390

ISSN: 2383-4536
jacm.scu.ac.ir

Shahid Chamran University of Ahvaz

Journal of Applied and Computational Mechanics

Research Paper

Surface Tension Modeling using the Axisymmetric Contact Smoothed Particle Hydrodynamics Method

Georgii Dmitrievich Rublev[1,2]

[1] Department of Mathematical Modeling, Dukhov Automatics Research Institute, Sushchevskaya St., 22, Moscow, 127030, Russia

[2] Laboratory of Physical Gas Dynamics, Joint Institute for High Temperatures of RAS, Izhorskaya st., 13, Bd. 2, Moscow, 125412, Russia

Received July 28 2025; Revised September 19 2025; Accepted for publication September 24 2025.
✉ Corresponding author: G.D. Rublev (rublev_gd_97@vk.com)

Abstract. This article demonstrates the possibilities of computer simulation of capillary phenomena using the axisymmetric contact smoothed particle hydrodynamics (CSPH) method. The conservation accuracy of total momentum and total energy is important in modeling of many physical problems, including capillary phenomena, since the non-physical acceleration may lead to incorrect deformation of free surfaces. A modified axisymmetric CSPH method is considered to improve the accuracy of preserving the total momentum and the total energy. An external pressure boundary condition is proposed for the CSPH method and used for surface tension modeling. The verification of the surface tension model is performed for three test cases: evaluating the Laplace pressure in a water droplet, estimating the period of small oscillations of a water droplet, and comparing the velocity of rims propagation driven by surface tension forces at thin film boundaries with Taylor-Culick's formula. A simulation of the Rayleigh-Plateau instability development is also conducted.

Keywords: Axisymmetric SPH, Contact SPH, Surface tension, Conservative schemes, Riemann solver.

1. Introduction

The meshless Smoothed Particle Hydrodynamics (SPH) method has a broad range of applications for modeling the mechanics of continuous media. In particular, it is well-suited for problems involving large deformations of free surfaces and material interfaces. The relative simplicity of its software implementation and the setup of boundary conditions along with the lack of need for complex mesh rebuilding, have contributed to the rapid growth in the popularity of the SPH method since its inception by Lucy [1] and Monaghan [2] in 1977. In subsequent years, numerous modifications of the SPH method have been proposed.

In 1999, Parshikov [3] presented the equations of the Contact Smoothed Particle Hydrodynamics (CSPH) method for the first time, wherein the interaction between contacting particles is treated using an approximate Riemann problem solution. In this sense, the CSPH method is analogous to the computation of fluxes through the cell edges in Godunov-type mesh-based methods [4]. The CSPH approach enables the elimination of artificial viscosity, the tuning of which may be rather sophisticated.

Three-dimensional modeling in a Cartesian coordinate system requires a large number of particles and can be computationally expensive, leading to prolonged simulation times. However, for a wide range of practical problems, two-dimensional axisymmetric modeling can be employed, which significantly accelerates the simulation process and reduces the computational cost. This study considers an axisymmetric variant of the CSPH method.

The axisymmetric smoothed particle hydrodynamics method was first proposed by Coleman and Bicknell in 1985 [5]. In 1993, Petschek [6] presented the axisymmetric variant of the SPH method, which was derived by the direct transformation of a three-dimensional Cartesian scheme with a Gaussian kernel into a two-dimensional axisymmetric one using angular integration. Subsequently, several alternative axisymmetric SPH methods have been proposed, which incorporate artificial viscosity (see, for example [7, 8]).

The axisymmetric CSPH method based on the Riemann problem solution was first proposed by Parshikov [9]. MUSCL reconstruction was incorporated into this scheme in [13] for simulation of ocean engineering problems. However, this scheme is not conservative. This is not only a consequence of the boundary condition setup, but also an inherent property of the equations themselves. Accurate conservation of the total momentum and the total energy is crucial when modeling many problems, including capillary phenomena, because unphysical acceleration may lead to incorrect evolution of free surfaces. To improve the conservation properties, this study provides a modified scheme for the axisymmetric CSPH method, where the total momentum and the total energy are exactly conserved in the absence of boundary conditions.

The SPH method with artificial viscosity is widely employed to simulate problems involving surface tension (see, for example [10-12]). In these studies, the surface tension is modeled by applying the force, which magnitude at surface particles is computed based on the curvature of the surface at them.

Published online: October 09 2025

In this work, a numerical boundary condition for the CSPH method is proposed, enabling the simulation of surface tension effects. The boundary particles interact with the ghost particles where pressure magnitude is equal to the Laplace pressure. This choice of numerical model for surface tension appears to be more optimal, as it allows the reduction of the noise level on the surface by adjusting the contribution to the SPH sums (weight) of the ghost particles. The paper is organized as follows: Section 2 provides a description of the axisymmetric CSPH method. Section 2.3 contains an explanation of the numerical surface tension model used. Finally, Section 3 presents the verification test results and simulation results for the development of Rayleigh-Plateau instability.

2. Axisymmetric Contact SPH Method

To describe compressible media in the axisymmetric case, the equations of continuity, motion, and energy are used. The continuity equation is more convenient to express in terms of volumetric deformation:

$$\frac{d\varepsilon}{dt} = -\frac{1}{\rho}\frac{d\rho}{dt} = \boldsymbol{\nabla}\cdot\boldsymbol{U} + \frac{U^r}{r}, \tag{1}$$

where $\nabla\cdot U = \frac{\partial U^r}{\partial r} + \frac{\partial U^z}{\partial z}$, $\nabla = (\partial/\partial r,\ \partial/\partial z)^{\mathrm{T}}$, $U = (U^r, U^z)^{\mathrm{T}}$ is velocity, ρ is the density.

Equation of motion is:

$$\frac{d\boldsymbol{U}}{dt} = -\frac{1}{\rho}\boldsymbol{\nabla}P + \frac{1}{\rho}\boldsymbol{f}^{\mathrm{st}}, \tag{2}$$

where P is the pressure and $\boldsymbol{f}^{\mathrm{st}}$ is the interfacial surface force. It is assumed that the surface tension coefficient σ is constant, hence, the Marangoni force has no influence on the interface dynamics. The fluid viscosity is assumed to be sufficiently small.

Using the previously introduced notation, the internal energy evolution equation is expressed as follows:

$$\frac{de}{dt} = -\frac{P}{\rho}\nabla\cdot U - \frac{PU^r}{\rho r}, \tag{3}$$

where e is the specific internal energy. Equations (1)-(3) are closed using an equation of state:

$$P = P(\rho, e).$$

The SPH method is based on the kernel approximation. In the axisymmetric case, for a function $F(r)$ it can be expressed as:

$$F(\boldsymbol{r}) = \int ds' F(\boldsymbol{r}')W(|\boldsymbol{r}-\boldsymbol{r}'|/h;h) + O(h^2), \tag{4}$$

where $ds' = dr'dz'$ is the area element. The smoothing kernel $W(q;h)$ is a function of $q = |r-r'|/h$ depending on the smoothing length h as a parameter. The smoothing length h is the support radius of the smoothing kernel function. Throughout this study, two-dimensional Wendland C^2 smoothing kernel function is used:

$$W(q;h) = \frac{7}{\pi h^2}\begin{cases}(1+4q)(1-q)^4, & 0 \le q \le 1,\\ 0, & q > 1,\end{cases}$$

$$W'(q;h) = \frac{dW}{dq}(q;h) = \frac{140}{\pi h^2}\begin{cases}q(1-q)^3, & 0 \le q \le 1,\\ 0, & q > 1.\end{cases}$$

After discretization, which represents the computational domain with particles, the continuous form of the kernel approximation (4) can be written via a summation of the neighboring particles as follows:

$$< F >_a = \sum_b F_b \frac{m_b}{2\pi r_b \rho_b} W_{ab}, \tag{5}$$

where m_a is the mass of a the a-th toroidal material element (SPH particle) of radius r_a. The particle size D_a is determined as $\sqrt{m_a/(2\pi\ r_a\rho_a)}$.

An estimate of the gradient $\boldsymbol{\nabla}F$ at point a can be written using Eq. (5):

$$< \boldsymbol{\nabla}F >_a = \sum_b F_b \frac{m_b}{2\pi r_b\rho_b}\boldsymbol{\nabla}_a W_{ab}, \tag{6}$$

where

$$\boldsymbol{\nabla}_a W_{ab} = -W'_{ab}\frac{\boldsymbol{e}^R_{ba}}{h_{ab}},$$

where $\boldsymbol{e}^R_{ba} = \frac{\boldsymbol{r}_b-\boldsymbol{r}_a}{|\boldsymbol{r}_b-\boldsymbol{r}_a|}$, $h_{ab} = \theta(D_a + D_b)$ is the smoothing length, θ is the smoothing length parameter. Traditionally the most frequently used values of θ in the CSPH are from 0.5 to 0.75, which is associated with acceptable performance. Throughout this article $\theta = 0.5$ is used.

Similarly for the vector field $\boldsymbol{F}$, one can write:

$$< \boldsymbol{\nabla}\cdot\boldsymbol{F} >_a = \sum_b \frac{m_b}{2\pi r_b\rho_b}\boldsymbol{F}_b\cdot\boldsymbol{\nabla}_a W_{ab}. \tag{7}$$

In the following, angle brackets are omitted when writing SPH approximations.

2.1. Axisymmetric CSPH method with enhanced conservation properties

The concept of the contact method CSPH involves incorporating the velocity and the pressure obtained from the solution of the Riemann problem on the contact surface into the SPH approximation, rather than utilizing the average values of velocity and pressure between pairs of interacting particles, as is conventional in SPH methods [3, 9].

The axisymmetric CSPH scheme of Parshikov [9] is:

$$\frac{d\varepsilon_a}{dt} = \sum_b \frac{m_b}{2\pi r_b \rho_b h_{ab}} 2(U_{ab}^{R*} - U_a^R) W'_{ab} + \frac{U_a^r}{r_a}, \tag{8}$$

$$\frac{d\boldsymbol{U}_a}{dt} = -\sum_b \frac{m_b}{2\pi r_b \rho_b \rho_a} 2P_{ab}^* \boldsymbol{\nabla}_a W_{ab}, \tag{9}$$

$$\frac{dE_a}{dt} = \sum_b \frac{m_b}{2\pi r_b \rho_b \rho_a} 2P_{ab}^* U_{ab}^{R*} W'_{ab} - \frac{P_a U_a^r}{r_a \rho_a}. \tag{10}$$

This scheme is not conservative even in the absence of boundary conditions. In this study, a modified axisymmetric CSPH scheme is used to improve the accuracy of preserving the total momentum and the total energy, which is called here as a harmonic mean (HM) scheme.

The HM scheme is derived using the following identities written at a point $\boldsymbol{r}$:

$$\boldsymbol{\nabla} P(\boldsymbol{r}) = \frac{\boldsymbol{\nabla}(f(r;r_0)P) + P\boldsymbol{\nabla} f(r;r_0)}{f(r;r_0)} - \frac{2P}{r+r_0}\boldsymbol{e}^r, \tag{11}$$

$$\boldsymbol{\nabla} \cdot \boldsymbol{U}(\boldsymbol{r}) = \frac{\boldsymbol{\nabla} \cdot (f(r;r_0)\boldsymbol{U}) - \boldsymbol{U} \cdot \boldsymbol{\nabla} f(r;r_0)}{f(r;r_0)}, \tag{12}$$

where $f(r;r_0) = (r+r_0)/2r_0$, r_0 is a certain radius, $\boldsymbol{e}^\alpha$, $\alpha = r, z$ are the unit basis vectors of the cylindrical coordinate system rz. It is worth mentioning that the function $f(r;r_0)$ can be chosen in different ways. For example, one can use $f(r;r_0) = \sqrt{r/r_0}$ or $f(r;r_0) = 2r/(r+r_0)$. A detailed comparison of different schemes has not been conducted, but their properties in terms of approximating equations are similar.

Using Eqs. (6) and (7) to approximate differential operators in identities (11) and (12), and assuming $r_0 = r_a$, the volumetric strain rate and acceleration at point $\boldsymbol{r}_a$ (i.e., for particle a) can be expressed as follows:

$$\frac{d\varepsilon_a}{dt} = \sum_b \frac{m_b}{2\pi\rho_b} \frac{r_a + r_b}{2r_a r_b} (\boldsymbol{U}_b - \boldsymbol{U}_a) \cdot \boldsymbol{\nabla}_a W_{ab} + \frac{U_a^r}{r_a}, \tag{13}$$

$$\frac{d\boldsymbol{U}_a}{dt} = -\sum_b \frac{m_b}{2\pi\rho_b\rho_a} \frac{r_a + r_b}{2r_a r_b} (P_a + P_b) \boldsymbol{\nabla}_a W_{ab} + \frac{P_a}{\rho_a r_a}\boldsymbol{e}^r. \tag{14}$$

The equation for internal energy evolution may be written as:

$$\frac{de_a}{dt} = -\sum_b \frac{m_b}{2\pi\rho_b\rho_a} \frac{r_a + r_b}{2r_a r_b} \frac{(P_a + P_b)}{2} (\boldsymbol{U}_b - \boldsymbol{U}_a) \cdot \boldsymbol{\nabla}_a W_{ab} - \frac{P_a U_a^r}{r_a \rho_a}.$$

Then the equation for the total energy takes the form:

$$\frac{dE_a}{dt} = \boldsymbol{U}_a \cdot \frac{d\boldsymbol{U}_a}{dt} + \frac{de_a}{dt} = -\sum_b \frac{m_b}{2\pi\rho_b\rho_a} \frac{r_a + r_b}{2r_a r_b} \frac{(P_a + P_b)}{2} (\boldsymbol{U}_b + \boldsymbol{U}_a) \cdot \boldsymbol{\nabla}_a W_{ab}. \tag{15}$$

Finally, after incorporating the solution of the Riemann problem into Eqs. (14), (13), and (15) the axisymmetric CSPH HM scheme is:

$$\frac{d\varepsilon_a}{dt} = -\sum_b \frac{m_b}{\pi\rho_b h_{ab}} \frac{r_a + r_b}{2r_a r_b} (U_{ab}^{R*} - U_a^R) W'_{ab} + \frac{U_a^r}{r_a}, \tag{16}$$

$$\frac{d\boldsymbol{U}_a}{dt} = -\sum_b \frac{m_b}{\pi\rho_b\rho_a} \frac{r_a + r_b}{2r_a r_b} P_{ab}^* \boldsymbol{\nabla}_a W_{ab} + \frac{P_a}{\rho_a r_a}\boldsymbol{e}^r. \tag{17}$$

$$\frac{dE_a}{dt} = -\sum_b \frac{m_b}{\pi\rho_b\rho_a h_{ab}} \frac{r_a + r_b}{2r_a r_b} P_{ab}^* U_{ab}^{R*} W'_{ab}, \tag{18}$$

where

$$P_{ab}^* = \frac{P_b Z_a + P_a Z_b - Z_a Z_b (U_b^R - U_a^R)}{Z_a + Z_b}, \tag{19}$$

$$U_{ab}^{R*} = \frac{U_a^R Z_a + U_b^R Z_b - P_b + P_a}{Z_a + Z_b}. \tag{20}$$

where $Z = C\rho$ is the acoustic impedance of the material and C is the speed of sound. U_{ab}^{R*} is the projection of the contact velocity between particles on the R-axis of the local coordinate system, RT (see Fig. 1). The R-axis connects the centers of the particles, and is directed from the point a to the point b. $\boldsymbol{e}_{ba}^R$ is the unit vector along R-axis. Since viscosity is not considered here, the Riemann problem is solved only along longitudinal (i.e., R) direction.

To reduce the numerical viscosity when modeling weakly compressible flows, equations of state with the artificial sound speed are used, see, for example [14, 15]). In this work the choice of artificial sound speed C_0 is based on maximal fluid flow speed U_{max}: $C_0 > 10U_{max}$. To maintain optimal particle packing, a particle shifting algorithm [16] is employed.

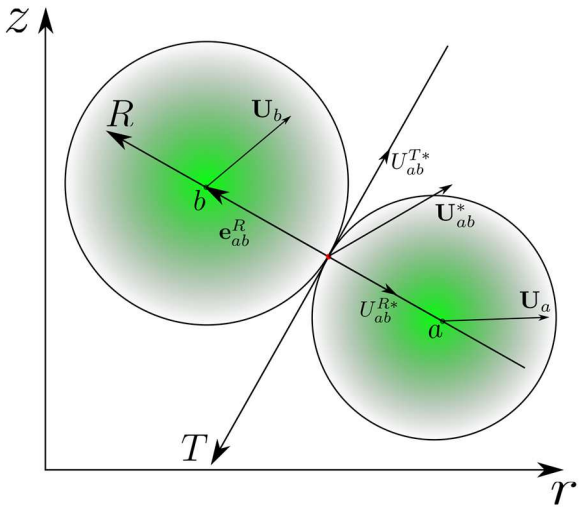

Fig. 1. Particle interaction in the local coordinate system RT.

The first-order scheme is used to integrate velocity, energy, and coordinates over time:

$$\boldsymbol{U}_a^{n+1} = \boldsymbol{U}_a^n + \left(\frac{d\boldsymbol{U}_a}{dt}\right)^n \Delta t^n, \qquad E_a^{n+1} = E_a^n + \left(\frac{dE_a}{dt}\right)^n \Delta t^n, \qquad \boldsymbol{r}_a^{n+1} = \boldsymbol{r}_a^n + \frac{1}{2}(\boldsymbol{U}_a^{n+1} + \boldsymbol{U}_a^n)\Delta t^n,$$

and for time integration of density the following scheme is used:

$$\rho_a^{n+1} = \rho_a^n \exp\left(\Delta t^n \left(\frac{d\varepsilon_a}{dt}\right)^n\right),$$

where $d\varepsilon_a/dt$ is determined by Eq. (16) (or by Eq. (8) in case of standard axisymmetric CSPH scheme of Parshikov). Current time step is calculated with the help of the Courant criterion:

$$\Delta t = \mathrm{CFL} \min_a \left(\frac{D_a}{\sqrt{C_a^2 + (4D_a d\varepsilon_a/dt)^2}}\right).$$

It is straightforward to observe that the total energy is exactly conserved in the HM scheme:

$$\frac{dE}{dt} = \sum_a \sum_b \frac{m_b}{\pi\rho_b\rho_a h_{ab}} \frac{r_a + r_b}{2r_a r_b} P_{ab}^* U_{ab}^{R*} W'_{ab} = \sum_a \sum_{b<a} \frac{m_b}{\pi\rho_b\rho_a h_{ab}} \frac{r_a + r_b}{2r_a r_b} P_{ab}^* (U_{ab}^{R*} + U_{ba}^{R*}) W'_{ab} = 0.$$

since the projection of the contact velocity U_{ab}^{R*} onto the axis R of the local coordinate system changes sign when the indices a and b are interchanged, i.e., when transitioning from the local coordinate system RT associated with particle a to the local coordinate system RT associated with particle b. For the same reason, the total momentum is also exactly conserved in the HM scheme.

2.2. Boundary condition near the axis of symmetry

For particles near the axis of symmetry the support radius of the smoothing kernel function is incomplete because there are no neighboring particles at $r < 0$. To solve this problem, it is necessary to introduce a special boundary condition by providing the ghost particles, which are obtained by the reflection of original particles across the symmetry axis, to the calculation of the SPH sums.

To comprehend the subsequent condition introduced near the axis of symmetry, it is necessary to clarify the behavior of the accuracy inherent in the proposed scheme in the vicinity of the axis. For this purpose, we first return to the smoothing stage and express the integrals evaluated using SPH summations in Eqs. (13)-(15). Specifically, for the continuity equation, we have:

$$-\int \frac{r_a + r}{2r_a}(\boldsymbol{U} - \boldsymbol{U}_a) \cdot \boldsymbol{\nabla} W\left(\frac{|\boldsymbol{r}_a - \boldsymbol{r}|}{h}; h\right) ds + \frac{U_a^r}{r_a} = \int \left(\frac{\boldsymbol{e}^r \cdot (\boldsymbol{U} - \boldsymbol{U}_a)}{2r_a} + \frac{r_a + r}{2r_a} \boldsymbol{\nabla} \cdot \boldsymbol{U}\right) W\left(\frac{|\boldsymbol{r}_a - \boldsymbol{r}|}{h}; h\right) ds + \frac{U_a^r}{r_a} =$$

$$\boldsymbol{\nabla} \cdot \boldsymbol{U}(\boldsymbol{r}_a) + O(h^2) = \frac{d\varepsilon}{dt}(\boldsymbol{r}_a) + O(h^2),$$

for the equation of motion, the same estimation is:

$$\frac{1}{\rho_a r_a} \int \frac{r_a + r}{2}(P_a + P) \boldsymbol{\nabla} W\left(\frac{|\boldsymbol{r}_a - \boldsymbol{r}|}{h}; h\right) ds + \frac{P_a \boldsymbol{e}^r}{\rho_a r_a} = -\frac{1}{\rho_a r_a} \int \left(\frac{(P_a + P)}{2} \boldsymbol{e}^r + \frac{r_a + r}{2} \boldsymbol{\nabla} P\right) W\left(\frac{|\boldsymbol{r}_a - \boldsymbol{r}|}{h}; h\right) ds + \frac{P_a \boldsymbol{e}^r}{\rho_a r_a} =$$

$$-\frac{1}{\rho_a r_a}\left(P_a \boldsymbol{e}^r + r_a \boldsymbol{\nabla} P(r_a) + O(h^2)\right) + \frac{P_a \boldsymbol{e}^r}{\rho_a r_a} = -\frac{1}{\rho_a} \boldsymbol{\nabla} P(\boldsymbol{r}_a) + \frac{1}{\rho_a r_a} O(h^2),$$

and for the energy equation, we have:

$$\frac{1}{\rho_a r_a} \int \frac{r_a + r}{2}(P_a + P)(\boldsymbol{U} + \boldsymbol{U}_a) \cdot \boldsymbol{\nabla} W\left(\frac{|\boldsymbol{r}_a - \boldsymbol{r}|}{h}; h\right) ds =$$

$$-\frac{1}{\rho_a r_a} \int \left[\left(\frac{(P_a + P)}{4} \boldsymbol{e}^r + \frac{r_a + r}{4} \boldsymbol{\nabla} P\right) \cdot (\boldsymbol{U} + \boldsymbol{U}_a) + \frac{r_a + r}{4}(P_a + P) \boldsymbol{\nabla} \cdot \boldsymbol{U}\right] W\left(\frac{|\boldsymbol{r}_a - \boldsymbol{r}|}{h}; h\right) ds =$$

$$-\frac{1}{\rho_a} \boldsymbol{\nabla} \cdot (P\boldsymbol{U})|_{\boldsymbol{r}=\boldsymbol{r}_a} - \frac{P_a U_a^r}{\rho_a r_a} + \frac{1}{\rho_a r_a} O(h^2).$$

It is evident from this that the approximation of the continuity equation exhibits no singularities near the axis of symmetry, whereas the error for the equations of motion and energy increases without bound as $r_a \to 0$. To ensure the smoothing error remains bounded, it is necessary to confine the applicability domain of the HM scheme; specifically, this scheme should only be applied to those particles for which $r > Kh$, where $K > 1$ is a constant. Under this condition, the maximum smoothing error will be of order $O(h)$.

Let's estimate the discretization error. For this purpose, results from the work of Quinlan et al. [18] can be used. Assuming the smoothness of the kernel function for irregularly packed particles, and accounting for the restriction of the scheme's applicability domain, it follows that the discretization error scales proportionally to $\frac{1}{h^2}(\frac{D}{h})^3$. Consequently, to prevent the approximation error from increasing as the smoothing length h decreases, it is necessary to simultaneously adjust both the smoothing length h and the ratio D/h of the particle size to the smoothing length. Unlike the standard SPH method, where D/h must decrease faster than $h^{1/3}$, the proposed HM scheme requires D/h to decrease faster than $h^{2/3}$. Such analysis is valid for gradient approximation, but it is difficult to analyze how it affects the results of a specific hydrodynamics simulation. The increase in discretization error with decrease of smoothing scale h at $D/h = \text{const}$ is well-known for the SPH method, but numerical experiments show that in many cases particles can be made sufficiently small without any problems with decreasing accuracy. So, the choice of the D/h ratio in the proposed scheme should be made manually for a specific problem as for other SPH schemes.

The axisymmetric Parshikov's [9] scheme (8)-(10) does not have singularity in the vicinity of the axis of symmetry and for this reason a local transition to this scheme is performed if $r < Kh$. Interactions with the ghost (reflected across the symmetry axis) particles are added to the SPH sums, and their velocities and coordinates should be properly transformed. Unfortunately, this violates the conservation laws for total energy and total momentum near the axis of symmetry.

To estimate how the boundary condition near the axis of symmetry affects the change in the total energy and the total momentum, the problem of collision of two water droplets of different sizes is considered. The initial radii of the droplets are 1 mm and 0.5 mm. The initial velocities of the droplets are 50 m/s and are oppositely directed along the z-axis. The initial size of SPH particles is 10 μm.

To model water, the Mie-Grüneisen equation of state with two reference curves is used:

$$P = P_{\text{ref}} + \gamma\rho(e - e_{\text{ref}}),$$

$$P_{\text{ref}} = \begin{cases} \dfrac{\rho_0 c_a^2(1-x)}{\left(1 - s_a(1-x)\right)^2}, & x \le 1, \\ \rho_0 c_a^2(1-x), & x > 0, \end{cases} \qquad e_{\text{ref}} = \begin{cases} \dfrac{1}{2}\left[\dfrac{c_a(1-x)}{1 - s_a(1-x)}\right]^2, & x \le 1, \\ c_a^2(1-x)^2/2, & x > 0, \end{cases}$$

where $x = \rho_0/\rho$, $\rho_0 = 1000$ kg/m^3, $c_a = 1483$ m/s, $s_a = 2$, $\gamma = 2$.

Figure 2 illustrates the evolution of the total momentum and the total energy using the axisymmetric CSPH HM scheme and Parshikov's axisymmetric CSPH scheme [9]. The results indicate that the HM scheme preserves the total momentum and the total energy much more accurately because, in general, it is conservative, and the introduced errors are of local character near the axis of symmetry.

2.3. Surface tension modeling

To model the surface tension, the ghost particles interacting with boundary particles are used. The ghost particles simulate the effect of external pressure, which is equal to the Laplace pressure. Each boundary particle and near boundary particle interacts with its own ghost particle. The algorithm for determining boundary particles is taken from [17]. The determination of boundary particles is based on the use of the minimum eigenvalue $\lambda_{\min}$ of the matrix:

$$\boldsymbol{L}_a = \sum_b \frac{m_b}{2\pi r_b \rho_b} \boldsymbol{\nabla}_a W_{ab} \otimes (\boldsymbol{r}_b - \boldsymbol{r}_a). \tag{21}$$

If for a particle $\lambda_{\min} < 0.75$, then it is considered as a boundary particle. In the axisymmetric case, a special boundary condition must be applied near the axis of symmetry to determine the boundary particles: for particles located near the axis, the contribution to the sum (21) comes not only from neighboring particles, but also from particles reflected across the axis of symmetry. A particle is considered to be near the boundary if there are boundary particles among its neighbors (within its smoothing length).

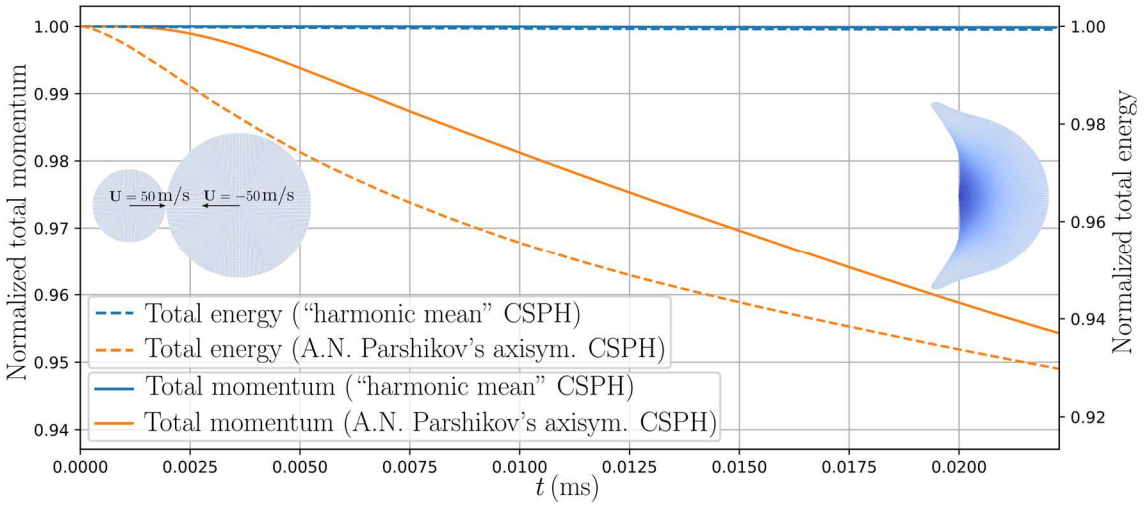

Fig. 2. Change in the total momentum and the total energy in the problem of collision of two water droplets using the axisymmetric CSPH scheme HM and the axisymmetric CSPH scheme of Parshikov [9].

Under constant pressure P_0 and in the absence of external forces, the acceleration should be zero. Based on this requirement, the weight of the ghost particles can be chosen. It should be selected such that the acceleration of the boundary particles equals zero when the internal pressure and pressure in the ghost particle are equal (let the pressure be P_0):

$$\frac{d\boldsymbol{U}_a}{dt} = -\sum_b \frac{m_b}{\pi\rho_b\rho_a}\frac{r_a+r_b}{2r_ar_b}P_0\boldsymbol{\nabla}_a W_{ab} + \frac{P_0}{\rho_a r_a}\boldsymbol{e}^r - \frac{1}{\rho_0}\boldsymbol{bw}_a 2P_0 = 0, \tag{22}$$

from which the weight vector for the ghost particle associated with a boundary particle a is given by:

$$\boldsymbol{bw}_a = -\sum_b \frac{m_b}{2\pi\rho_b}\frac{r_a+r_b}{2r_ar_b}\boldsymbol{\nabla}_a W_{ab} + \frac{\boldsymbol{e}^r}{2r_a}. \tag{23}$$

In the region where scheme (8)-(10) is applied, the weight vector is:

$$\boldsymbol{bw}_a = -\sum_b \frac{m_b}{2\pi\rho_b r_b}\boldsymbol{\nabla}_a W_{ab}\,.$$

The interaction between the ghost particle g and the boundary particle a is implemented as follows:

$$\frac{d\varepsilon_a}{dt} = -\sum_b \frac{m_b}{\pi\rho_b h_{ab}}\frac{r_a+r_b}{2r_ar_b}(U_{ab}^{R*}-U_a^R)W'_{ab} + \frac{U_a^r}{r_a} + 2(U_{ag}^{R*}-U_a^R)|\boldsymbol{bw}_a|, \tag{24}$$

$$\frac{d\boldsymbol{U}_a}{dt} = -\sum_b \frac{m_b}{\pi\rho_b\rho_a}\frac{r_a+r_b}{2r_ar_b}P_{ab}^*\boldsymbol{\nabla}_a W_{ab} + \frac{P_a}{\rho_a r_a}\boldsymbol{e}^r - \frac{2P_{ag}^*}{\rho_a}\boldsymbol{bw}_a, \tag{25}$$

$$\frac{dE_a}{dt} = -\sum_b \frac{m_b}{\pi\rho_b\rho_a h_{ab}}\frac{r_a+r_b}{2r_ar_b}P_{ab}^*U_{ab}^{R*}W'_{ab} - \frac{2P_{ag}^*}{\rho_a}U_{ag}^{R*}|\boldsymbol{bw}_a|, \tag{26}$$

When interacting with a ghost particle (the last terms in Eqs. (24)-(26)), the unit vector along the *R* axis of the local coordinate system is defined as $\boldsymbol{e}_{ag}^R = -\boldsymbol{bw}_a/|\boldsymbol{bw}_a|$. The pressure in a ghost particle is set equal to the Laplace pressure P_L, and the velocity is set equal to the velocity of boundary particle a. The acoustic impedance of the ghost particle should be set based on physical formulation of a specific problem. In this work to simulate surface tension the acoustic impedance of ghost particles is set as for low density (approximately vacuum) media. For this purpose, the acoustic impedance Z_g of ghost particles is set six orders of magnitude less than the acoustic impedance Z_a of corresponding real particles. According to Eq. (19), the pressure at the free surface (i.e. contact pressure P_{ag}^*) is $P_{ag}^* \approx P_L$ and therefore the proposed algorithm approximates boundary condition on free surface to model surface tension.

To determine the curvature κ and the outward normal, an algorithm from Ref. [12] is used. The vector of the outward normal to the free surface is defined as:

$$\boldsymbol{n}_a = \frac{\boldsymbol{\nu}_a}{|\boldsymbol{\nu}_a|},$$

$$\boldsymbol{\nu}_a = \sum_b \frac{m_b}{2\pi r_b\rho_b}\boldsymbol{\nabla}_a W_{ab}\,.$$

The curvature is calculated as:

$$\kappa = 2\frac{\sum_b \frac{m_b}{2\pi r_b\rho_b}(\boldsymbol{n}_b-\boldsymbol{n}_a)\cdot\boldsymbol{\nabla}_a W_{ab}}{\sum_b \frac{m_b}{2\pi r_b\rho_b}(\boldsymbol{r}_b-\boldsymbol{r}_a)\cdot\boldsymbol{\nabla}_a W_{ab}} + \frac{n_a^r}{r_a},$$

where n^r denotes the radial component of the outward normal vector to the free surface. To improve the accuracy of the curvature estimate, the normal n is computed using an increased smoothing length (i.e., the smoothing length parameter θ is set from 1 to 1.5, depending on the spatial discretization accuracy). The Laplace pressure is given by $P_L = \sigma\kappa$, where σ is the surface tension coefficient.

The described approach for surface tension modeling is not conservative. However, it is possible to improve it by calculating the resulting force from all ghost particles, acting on boundary particles:

$$\Delta F^z = \sum_a m_a \frac{2P_{ag}^*}{\rho_a}(bw_a)^z$$

and correcting the momentum of the boundary particles, which interacts with ghost particles. For this purpose, the following modification of the time integration scheme for z-component of velocity is used:

$$(U_a^{n+1})^z = (U_a^n)^z + \left(\frac{dU_a^z}{dt}\right)^n \Delta t^n - \frac{\Delta F_n^z}{m_{tot}}\Delta t^n,$$

where $m_{tot} = \sum_a m_a$ is total particle mass. In this case, conservation of the total momentum is managed only by the choice of axisymmetric SPH scheme. To demonstrate the effect of the momentum correction when employing the surface tension model, the test involving the collision of two water droplets (diameters 0.1 mm and 0.15 mm) was conducted. This test compares the performance of the proposed axisymmetric CSPH HM scheme, featuring improved conservation properties, against the standard axisymmetric CSPH scheme. The parameter K = 2, the time integration if performed with CFL = 0.5, the smoothing length parameter $\theta = 0.5$, the initial particle size is 1.1 μm. The linear equation of state is used for the simulation $P = C_0^2(\rho-\rho_0)$, where the initial density $\rho_0 = 1000$ kg/m^3 and C_0 is the artificial sound speed ($C_0 = 240$ m/s). Surface tension coefficient is $\sigma = 0.074$ N/m. The results are shown in Fig. 3. When employing the proposed scheme, the change in total momentum did not exceed 0.005%. In contrast, the use of the standard axisymmetric CSPH method by A.N. Parshikov provides the total momentum loss more than 3.5%.

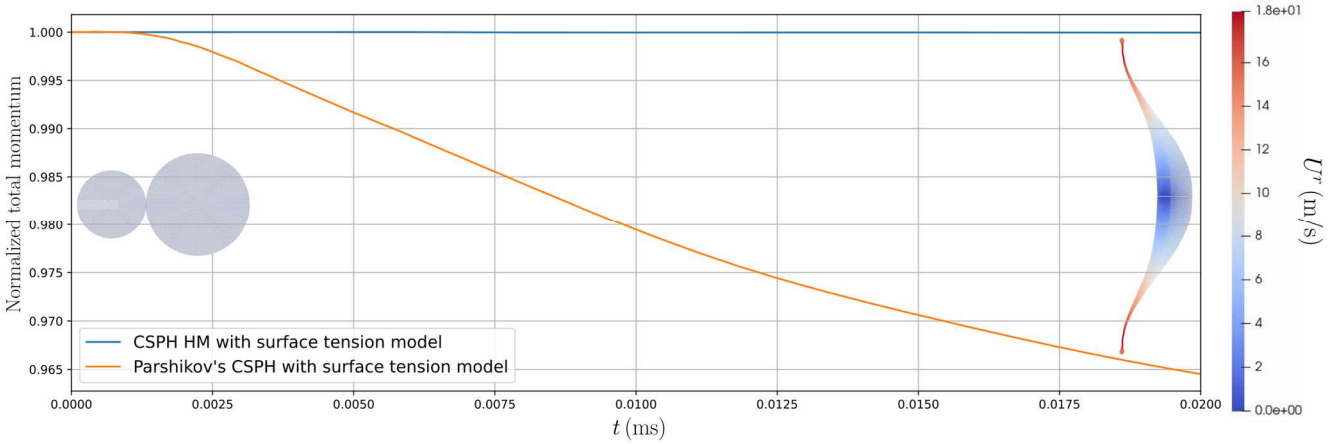

Fig. 3. Change in the total momentum in the problem of collision of two water droplets using the axisymmetric CSPH scheme HM and the standard axisymmetric CSPH scheme of Parshikov [9] with surface tension model and momentum correction.

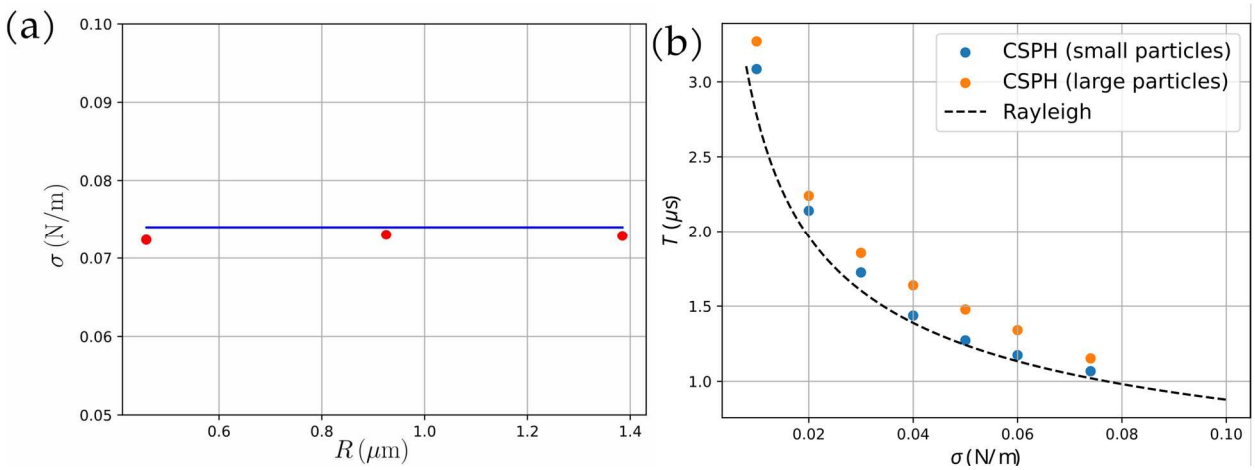

Fig. 4. (a) Comparison of the surface tension coefficient σ calculated from the established pressure in a water droplet with the given surface tension value, (b) Dependence of the period of the water droplet oscillations on the surface tension coefficient σ. Comparison with Rayleigh's formula.

It should be noted that such correction is feasible because, at each time step, the resultant force exerted by ghost particles on real particles at the boundary can be computed, and the momentum imbalance introduced into the total momentum by the surface tension model can be determined. In contrast, it is impossible to similarly correct for the influence of the intrinsic non-conservativity of the SPH scheme itself. This limitation arises because the simulated system may not be closed in the general case (e.g., external force fields may be present), making it impossible to disentangle changes in total momentum attributable to genuine physical effects from those arising due to the scheme's non-conservative properties.

3. Numerical Examples

3.1. Establishment of Laplace pressure in a water droplet

A fundamental test of the surface tension model is the test of establishing the Laplace pressure corresponding to a given surface tension coefficient. The excess pressure under the curved surface of a spherical droplet, according to the Laplace formula, is as follows:

$$P = \frac{2\sigma}{R}, \tag{27}$$

where R is the droplet radius. Figure 4(a) shows the obtained value of the surface tension coefficient calculated using formula (27) from the simulation results of the axisymmetric CSPH HM method with the proposed surface tension model. Particles with size $D = 28$ nm are used. The material of the droplet is water, and the surface tension coefficient is set to $\sigma = 0.074$ N/m. The linear equation of state is used for the simulation:

$$P = C_0^2(\rho - \rho_0),$$

where $C_0 = 1483$ m/s, $\rho_0 = 1000$ kg/m^3. The obtained results are in good agreement with the Laplace formula.

3.2. Small oscillations of a water droplet

This test is aimed to demonstrate the accuracy of the surface tension model for dynamic problems. The period of small droplet oscillations is determined by the Rayleigh's formula [19]:

$$T = 2\pi\sqrt{\frac{\rho R^3}{8\sigma}}, \tag{28}$$

where R is equilibrium droplet radius, ρ is density of the droplet material.

Table 1. Parameters and results in the problem of retracting a thin film with free boundaries under surface tension.

ΔH, μm	U_{TC}, m/s	U_{TC}^{SPH}, m/s	Initial outer radius R_{init}^{out}, m	Initial particle size D, nm
0.5	17.20	17.17	1.000001	20
1.5	7.92	7.48	1.000003	30

Water droplet with diameter $d = 5$ μm is considered. Initially, the following velocity field is set in the droplet:

$$U^r = \frac{r}{R}\left(1 - \frac{z^2}{R\sqrt{r^2+z^2}}\right)\exp\left(-\frac{\sqrt{r^2+z^2}}{R}\right),$$

$$U^z = -\frac{z}{R}\left(1 - \frac{r^2}{R\sqrt{r^2+z^2}}\right)\exp\left(-\frac{\sqrt{r^2+z^2}}{R}\right).$$

For simulation the linear equation of state is used with artificial sound speed $C_0 = 150$ m/s (this value was selected to achieve a sufficiently low numerical viscosity while maintaining the stability of the solution). Two series of numerical experiments were conducted: with initial SPH-particle size $D = 71.4$ nm (large particles) and $D = 35.7$ nm (small particles). In the first instance, the droplet radius accommodated 70 particles, whereas in the second instance, it accommodated 140 particles. For time integration, $\mathrm{CFL} = 0.3$ is used, the smoothing length parameter is $\theta = 0.5$ and parameter $K = 2$.

In Fig. 4(b), the dependence of the oscillation period of the droplet using the axisymmetric CSPH HM scheme is shown in comparison with Eq. (28). The obtained periods of small droplet oscillations are in good agreement with Rayleigh's formula. A slight increase in the period is due to the effect of the numerical viscosity: the smaller particles the smaller numerical viscosity and obtained periods closer to Eq. (28). At small values of the surface tension coefficient, the effect of the numerical viscosity on the period is maximal.

3.3. Taylor-Culick speed

The problem of a thin film with free boundaries retracting under surface tension forces is considered. The material is water, with the linear equation of state, where the artificial sound speed $C_0 = 200$ m/s. The velocity of the disturbance moving from the boundary (the point of transition from the film to the rim formed by surface tension) depends on the film thickness and the surface tension coefficient, and is determined by the Taylor-Culick formula [20]:

$$U_{TC} = \sqrt{\frac{2\sigma}{\rho \Delta H}}.$$

In the calculation, films with thicknesses of $\Delta H = 0.5$ μm and $\Delta H = 1.5$ μm are considered. The total number of particles in these two cases is 12500 and 75000. Initial inner radius of the film is chosen equal to 1 m to make curvature on the edges in angular direction negligible. The parameters used in simulations and the results are presented in Table 1. For time integration $\mathrm{CFL} = 0.3$ is used, the smoothing length parameter $\theta = 0.5$. There are no particles near the axis so parameter K is not important. Figure 5 shows the results of the simulations using the axisymmetric CSPH HM scheme of these two test cases. The results demonstrate the applicability of the proposed surface tension model for simulating dynamic problems with complex geometries.

In the current implementation of the code, the mean time expenditure per particle at each step amounted to 3.8 microseconds in this problem. This performance was attained utilizing 8 cores of an AMD Ryzen 7 processor. The results may vary depending on the software implementation and the hardware used.

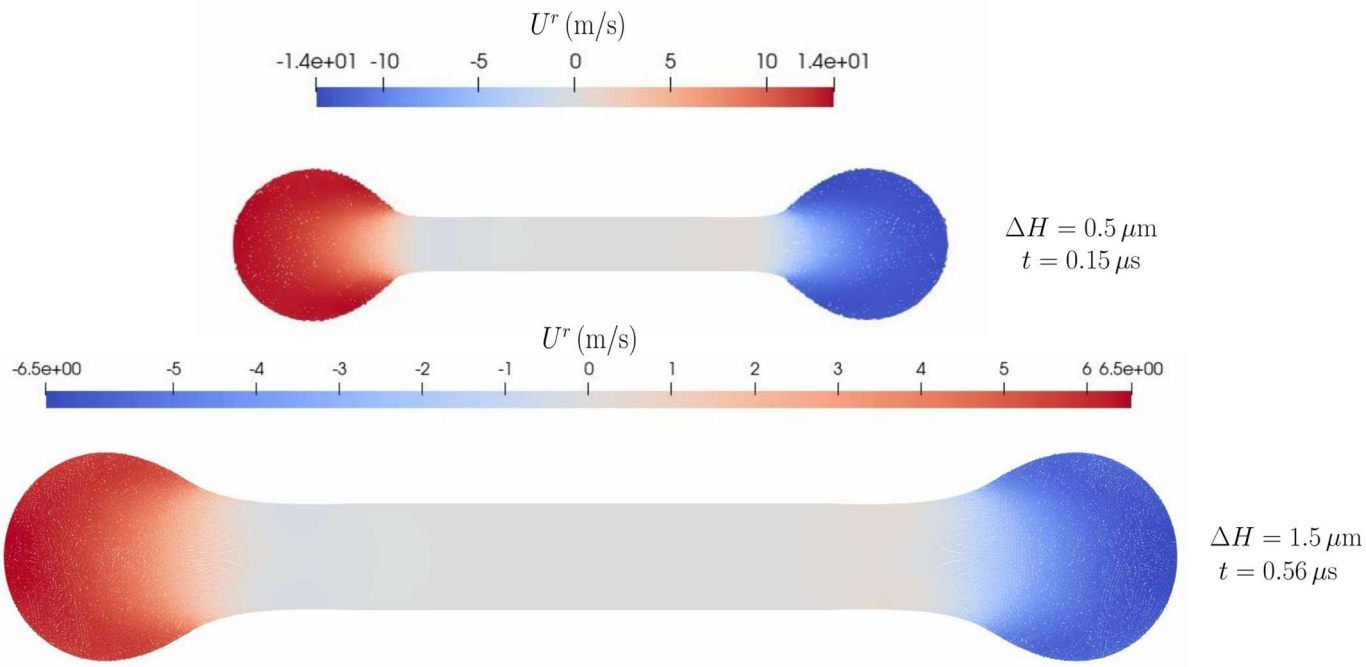

Fig. 5. Action of the surface tension forces on the boundaries of a thin flat film: axisymmetric simulation results.

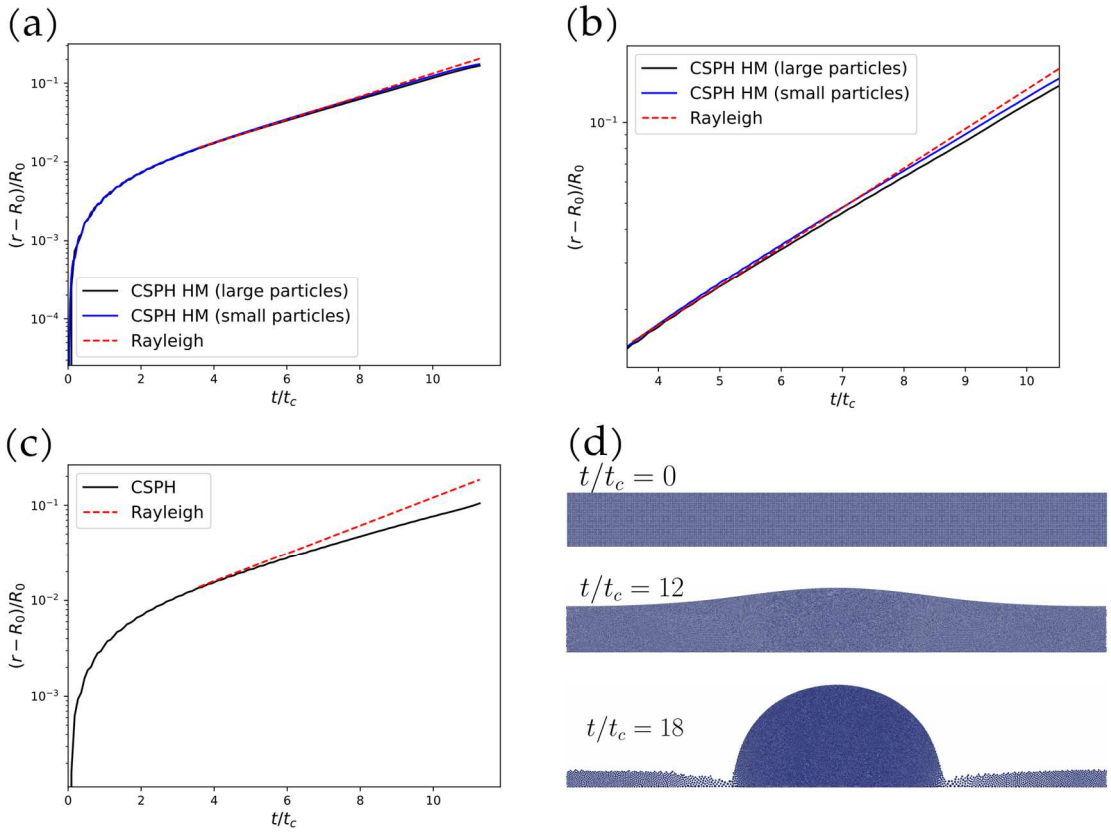

Fig. 6. Rayleigh-Plateau instability development: (a), (b), (d) Simulation results of instability development using proposed axisymmetric CSPH HM scheme with different resolution, (c) Simulation results of instability development using standard Parshikov's axisymmetric CSPH scheme.

3.4. Simulation of the Rayleigh-Plateau instability development

A cylindrical water jet is considered under periodic boundary conditions with a small initial velocity disturbance. The initial radius is $R_0 = 1$ μm. The disturbance wavelength is $\lambda = 10R_0$ and the wavenumber is $kR_0 = 2\pi/10$. The velocity disturbance used is:

$$U^z = U_0 \sin(2\pi z/\lambda)\,,$$

where $U_0 = 0.1$ m/s. Since the problem can be simulated under weakly compressible assumption, the water is modeled using the linear equation of state with artificial sound speed $C_0 = 80$ m/s.

Because the study of the numerical viscosity properties of the axisymmetric CSPH method is not the purpose of this work, the consideration is limited by the linear theory of capillary instability of inviscid liquid jets. According to Rayleigh's work [21], the growth rate of disturbances ($r \propto \exp(qt)$) is determined by the following formula:

$$q^2 = \frac{\sigma}{\rho R_0^3}\frac{I_1(kR_0)}{I_0(kR_0)}kR_0(1-(kR_0)^2).$$

The characteristic time is $t_c = \sqrt{\rho R_0^3/\sigma} = 0.116\ \mu s$. Figure 6 shows the development of Rayleigh-Plateau instability in a cylindrical jet based on the simulation results using the axisymmetric CSPH HM scheme with two different initial particle sizes ($D = 16.67$ nm (36000 particles) and $D = 8.3$ nm (144000 particles)) and the standard axisymmetric CSPH scheme (8)-(10) (with initial particle size $D = 16.67$ nm (36000 particles)). Here the mean time expenditure per particle at each step amounted to 3.75 microseconds (this performance was attained utilizing 8 cores of an AMD Ryzen 7 processor), which is approximately the same as in the previous case of the Taylor-Culick problem. At a time $t/t_c \approx 3.5$, a transition to exponential growth occurs. The growth rate of the disturbances is close to Rayleigh's estimate, but the numerical curve is slightly lower, which is a consequence of the presence of numerical viscosity. In Figs. 6(a) and 6(b), a comparison between the evolution of the central droplet radius obtained with proposed CSPH HM method and Rayleigh's formula is shown. Figure 6(b) demonstrates zoomed in section with exponential growth of disturbances (i.e., initial stage of the Rayleigh-Plateau instability development). Simulation with smaller particles lead to a result much closer to the Rayleigh's formula, which is associated with smaller numerical viscosity. Figure 6(c) demonstrates results obtained with the standard axisymmetric CSPH scheme. The results without the proposed modifications are worse, which indicates a decrease in the error rate due to improved accuracy in preserving total momentum and total energy.

4. Conclusion

In this study, the axisymmetric contact SPH method with improved conservation properties of the total momentum and the total energy (the HM scheme) is considered. In the general case, near the axis of symmetry, a special boundary condition for SPH particles is applied, which violates the exact conservation of the total energy and the total momentum. As soon as there is a rather small number of particles near the axis of symmetry, the numerical (i.e., non-physical) change in the total momentum and the total energy is significantly smaller than in the earlier axisymmetric scheme of Parshikov [9]. A surface tension model is introduced to the axisymmetric contact SPH method with the HM scheme. The surface tension model is implemented using the ghost particles interacting with the boundary particles near the free surface. The proposed numerical model for simulating compressible fluid

flows with surface tension is verified for problems such as the establishment of Laplace pressure, small oscillations of a droplet, and retraction of a thin film by surface tension. The obtained results are in good agreement with the theoretical estimates. A simulation of the Rayleigh-Plateau instability development is also performed. Despite the good results, the proposed model for simulating surface tension requires an extension to the case of contact between two different liquids. At the moment it is the main constraint of the proposed model. In this work the physical viscosity is not modeled: an approach similar to the proposed in [22] can be used, but it requires an analysis of the numerical viscosity of the axisymmetric CSPH method, which is not considered in this work.

Author Contributions

G.D. Rublev developed, implemented and validated the scheme. G.D. Rublev wrote the whole manuscript.

Acknowledgments

The author expresses his gratitude to S.A. Dyachkov, S.Yu. Grigoryev and Prof. V.V. Zhakhovsky for their helpful comments and suggestions.

Conflict of Interest

The author declared no potential conflicts of interest concerning the research, authorship, and publication of this article.

Funding

This work was supported by the Ministry of Science and Higher Education of the Russian Federation under Grant number 075-00269-25-00.

Data Availability Statements

Not applicable.

Code Availability

The article uses in-house code that cannot be made publicly available or sent by request.

References

[1] Lucy, L., A numerical approach to the testing of the fission hypothesis, *The Astronomical Journal*, 82(12), 1977, 1013–1024.
[2] Gingold, R.A., Monaghan, J.J., Smoothed particle hydrodynamics: theory and application to non-spherical stars, *Monthly Notices of the Royal Astronomical Society*, 181(3), 1977, 375–389.
[3] Parshikov, A.N., Application of a solution to the Riemann problem in the SPH method, *Zhurnal Vychislitel'noi Matematiki i Matematicheskoi Fiziki*, 39(7), 1999, 1216–1225.
[4] Toro, E., *Riemann Solvers and Numerical Methods for Fluid Dynamics*, Springer Berlin, 2013.
[5] Coleman, C., Bicknell, G.V., Jets with entrained clouds – I. hydrodynamic simulations and magnetic field structure, *Monthly Notices of the Royal Astronomical Society*, 214, 1985, 337–355.
[6] Petschek, A., Libersky, L., Cylindrical smoothed particle hydrodynamics, *Journal of Computational Physics*, 109, 1993, 76–83.
[7] Omang, M., Børve, S., Trulsen, J., SPH in spherical and cylindrical coordinates, *Journal of Computational Physics*, 213(1), 2006, 391–412.
[8] Li, M.-K., Zhang, A.-M., Ming, F.-R., Sun, P.-N., Peng, Y.-X., An axisymmetric multiphase sph model for the simulation of rising bubble, *Computer Methods in Applied Mechanics and Engineering*, 366, 2020, 113039.
[9] Parshikov, A.N., Medin, S.A., Loukashenko, I.I., Milekhin, V.A., Improvements in sph method by means of interparticle contact algorithm and analysis of perforation tests at moderate projectile velocities, *International Journal of Impact Engineering*, 24, 2000, 779–796.
[10] Morris, J.P., Simulating surface tension with smoothed particle hydrodynamics, *International Journal for Numerical Methods in Fluids*, 33, 2000, 333–353.
[11] Hu, X.Y., Adams, N.A., A multi-phase SPH method for macroscopic and mesoscopic flows, *Journal of Computational Physics*, 213, 2006, 844–861.
[12] Adami, S., Hu, X., Adams, N., A new surface-tension formulation for multi-phase SPH using a reproducing divergence approximation, *Journal of Computational Physics*, 229, 2010, 5011–5021.
[13] Fang, X.-L., Colagrossi, A., Wang, P.-P., Zhang, A.-M., An accurate and robust axisymmetric SPH method based on Riemann solver with applications in ocean engineering, *Ocean Engineering*, 244, 2022, 110369.
[14] Sun, P.N., Colagrossi, A., Marrone, S., Zhang, A.M., The δ^+-SPH model: Simple procedures for a further improvement of the SPH scheme, *Computer Methods in Applied Mechanics and Engineering*, 315, 2017, 25-49.
[15] Ren, Y., Lin, P., Zhang, C., Hu, X., An efficient correction method in Riemann SPH for the simulation of general free surface flows, *Computer Methods in Applied Mechanics and Engineering*, 417, 2023, 116460.
[16] Michel, J., Vergnaud, A., Oger, G., Hermange, C., Touze, D.L., On particle shifting techniques (PSTs): Analysis of existing laws and proposition of a convergent multi-invariant law, *Journal of Computational Physics*, 459, 2022, 110999.
[17] Marrone, S., Colagrossi, A., Le Touzé, D., Graziani, G., Fast free-surface detection and level-set function definition in SPH solvers, *Journal of Computational Physics*, 229, 2010, 3652–3663.
[18] Quinlan, N.J., Basa, M., Lastiwka, M.M., Truncation error in mesh-free particle methods, *International Journal for Numerical Methods in Engineering*, 66, 2006, 2064-2085.
[19] Reyleigh, L., On the capillary phenomena of jets, *Proceedings of the Royal Society*, 29, 1879, 71–97.
[20] Taylor, G.I.S., The dynamics of thin sheets of fluid. II. waves on fluid sheets, *Proceedings of the Royal Society of London. Series A. Mathematical and Physical Sciences*, 253, 1959, 296–312.
[21] Reyleigh, L., On the instability of jets, *Proceedings of the London Mathematical Society*, 10, 1878, 4–13.
[22] Parshikov, A., Medin, S., Rublev, G., Dyachkov, S., Numerical viscosity control in Godunov-like smoothed particle hydrodynamics for realistic flows modeling, *Physics of Fluids*, 36, 2024, 013101.

ORCID iD

Georgii D. Rublev https://orcid.org/0009-0008-5616-2355

How to cite this article: Rublev G.D. Surface Tension Modeling using the Axisymmetric Contact Smoothed Particle Hydrodynamics Method, *J. Appl. Comput. Mech.*, 12(3), 2026, 759-769. https://doi.org/10.22055/jacm.2025.48645.5390